Introduction of Asymmetry to Enhance Thermal Transport in Porous Metamaterials at Low Temperature

Yu Yang(杨宇), Dengke Ma(马登科), and Lifa Zhang(张力发)*

Phonon Engineering Research Center of Jiangsu Province, Center for Quantum Transport and Thermal Energy Science, Institute of Physics Frontiers and Interdisciplinary Sciences, School of Physics and Technology, Nanjing Normal University, Nanjing 210023, China

(Received 30 August 2023; accepted manuscript online 3 November 2023)

Introducing porosity with different degrees of disorder has been widely used to regulate thermal properties of materials, which generally results in decrease of thermal conductivity. We investigate the thermal conductivity of porous metamaterials in the ballistic transport region by using the Lorentz gas model. It is found that the introduction of asymmetry and Gaussian disorder into porous metamaterials can lead to a strong enhancement of thermal conductivity. By dividing the transport process into ballistic transport, non-ballistic transport, and unsuccessful transport processes, we find that the enhancement of thermal conductivity originates from the significant increase ballistic transport ratio. The findings enhance the understanding of ballistic thermal transport in porous materials and may facilitate designs of high-performance porous thermal metamaterials.

DOI: 10.1088/0256-307X/40/12/124401

In recent years, with the continuous development of micro–nanoscale industrial processing technologies, high integration has become an important trend. This progress has led to an urgent and multi-scenario demand for accurate thermal control.[1] Therefore, researchers have proposed a variety of strategies[2–4] to address the diverse thermal management requirements from macro[5–7] to micro scales.[8–13] Among these thermal management strategies, thermal metamaterials,[3–5] especially porous thermal metamaterials,[14–31] have attracted wide attention due to their low lab-fabrication difficulty and rich physical properties.

In general, introduction of pores into a material can cause a strong phonon interference effect,[14–16] resulting in a significant reduction in the thermal conductivity.[17–22] This phenomenon is strongly enhanced as the pores become disordered.[22–29] However, several recent results have challenged this conventional understanding.[30–32] Maire *et al.* demonstrated an abnormal enhancement of thermal conductivity by introducing disordered pores into silicon-on-insulator wafer at 4 K.[30] They attribute this to the fact that disorder reduces the cut-off frequency imposed by the phononic crystals, which increases the number of phonons propagating in the materials. Due to the extremely large number of disordered configurations, this phenomenon was not found again in subsequent molecular dynamics studies. Since then, it was not until Wei *et al.* used a search algorithm that combined a genetic algorithm and the Boltzmann transport equation to find several special configurations with abnormally enhanced thermal conductivity in porous monolayer graphene at 300 K.[31] However, the difference here is that all disorder configurations should have broken the phonon bandgap, but only a few configurations showed abnormal enhancement of thermal conductivity. The abnormal enhancement in thermal conductivity in porous graphene is explained by the particular pore arrangement that enhances the transport of particle-like phonons. More recently, we also found abnormally enhanced thermal conductivity in macro-systems at room temperature and correlated this phenomenon to the mean local angle of the thermal flux.[32]

Due to the difficulty of considering quantum effects at low temperature in conventional molecular dynamics methods, the abnormal enhancement of thermal conductivity at low temperature has rarely been studied. Compared with the high-temperature case, the scattering between phonons is obviously weakened at low temperature. In this case, the scattering caused by the porous structure may dominate the mean-free path of phonons and, under special circumstances, a ballistic transport process may even occur in the system. Therefore, in this work, we use the Lorentz gas model without considering the interaction between particles to study the ballistic thermal transport in porous metamaterials.

The traditional Lorentz gas model, which is a single-particle transport system regardless of interactions between particles, was originally used by Lorentz to describe the motion of an electron in metal.[33] Subsequently, various types of scatters, the interaction between particles, temperature reservoirs, and chemical potential reservoirs were gradually introduced into the Lorentz gas model. This led to the exploration of the rich physical properties of various systems in equilibrium[34–37] and non-equilibrium states.[38–48] In general, the Lorentz gas model has good

*Corresponding author. Email: phyzlf@njnu.edu.cn
© 2023 Chinese Physical Society and IOP Publishing Ltd

tunability, thus showing good reproducibility and the ability to provide a clear physical interpretation in many thermal transport problems, especially weakly interacting systems. Therefore, we choose the Lorentz gas model to study the thermal transport process in the ballistic porous system.

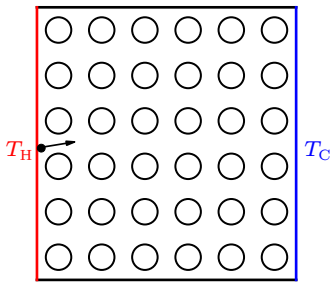

Fig. 1. Schematic diagram of the porous metamaterial model with the uniform porous configuration. The outline of the porous metamaterial model is a square with sides of 60, and the particle moves in the region outside the circle pores. The radius of the circular pore is set to 3. The left and right ends of the model are the isothermal thermal reservoirs with the temperature $T_{\rm H} = 2$ and $T_{\rm C} = 1$, respectively. In this study, the x and y directions are set parallel and perpendicular to the thermal transport direction, respectively.

The schematic diagram of a porous metamaterial for the Lorentz gas model is shown in Fig. 1, where 36 circles of radius $r = 3$ are uniformly arranged in a two-dimensional porous sheet with a square side length of $a = 60$. Two thermal reservoirs with temperature $T_{\rm H} = 2$ and $T_{\rm C} = 1$ are placed at the left and right ends of the model. For simplicity, in this study, we employ dimensionless units and set the Boltzmann constant $k_{\rm B}$ and the mass of the particle m to 1. Initially, a particle is randomly generated in the thermal reservoir and emitted into the model with a random velocity. The velocity distribution of particle is closely related to the temperature of the thermal reservoir. Its velocity distribution is as follows:

$$P(v_x) = \frac{|v_x|}{T_i} e^{-v_x^2/(2T_i)}, \tag{1}$$

$$P(v_y) = \frac{1}{\sqrt{2\pi T_i}} e^{-v_y^2/(2T_i)}. \tag{2}$$

Here, v_x and v_y represent the velocity components perpendicular to and parallel to the thermal reservoir, and T_i represents the temperature of the thermal reservoir from which the particle is emitted. In particular, when a particle is emitted by one thermal reservoir, its velocity v_x is always towards the inside of the model, which means that v_x is always positive when the particle is emitted from the hot reservoir, and *vice versa*. Subsequently, the particle moves continuously in the model, colliding elastically with the boundaries of the model and the circular pore structure, until the particle reaches and is absorbed into either the hot reservoir or the cold reservoir. Then, the thermal reservoir that absorbs the particle will produce another particle incident into the model at a random location according to Eqs. (1) and (2). This process will circulate continuously until the energy flux from the hot reservoir to the cold reservoir reach stability.

We now turn to define two quantities, local temperature and thermal flux, which are closely related to thermal transport.[40–48] We divide the model space into a series of boxes $\{m\}$ along the direction parallel to the boundary of the thermal reservoir. The crossing time and energy of each particle visiting the box m are recorded, so the average energy of the particle in box m can be obtained. Due to the equipartition theorem and the non-interacting premise, the average kinetic energy in the box m is considered to be proportional to its temperature, so the temperature in box m can be given by

$$T_m = \frac{2}{3} E_m, \tag{3}$$

where T_m and E_m represent the temperature and average kinetic energy of the box m, respectively. In Fig. S1 of the Supplementary Material, we give the temperature distribution along the transport direction. The temperature distribution remains constant in the open space between the circular porous structure, because the particle is not scattered in this region. Therefrom, ballistic transport occurs and the system does not satisfy Fourier's law. Since only the energy of the particle changes when it collides with the thermal reservoir, the thermal flux can be defined as

$$J = \frac{\Delta E}{t}, \tag{4}$$

$$\Delta E = \left| E^{\rm absorbed} - E^{\rm released} \right|, \tag{5}$$

where ΔE and t represent the absolute value of the change in energy for any reservoir and the total simulation time. Naturally, the effective thermal conductivity (ETC) of the porous metamaterial model can be defined as

$$\mathrm{ETC} = \frac{JL}{(T_{\rm H} - T_{\rm C})D}, \tag{6}$$

where L and D represent the length and width of the model, respectively. In this work, all parameters are subjected to a long-time statistical average to minimize their statistical fluctuations.

The ETC of various-ordered porous configurations is initially studied and their geometry is shown in Fig. 2(a). A total of 10 configurations can be divided into two classes: the ordered porous configurations constructed in the x direction and the y direction. We named each structure according to the clustering form of the pores. For example, $X(2|2|2)$ indicates that the pores are divided into three groups in the x direction and two pores in each group form the cluster block, which together constitute an ordered configuration. Since the particle experiences specular reflection at the upper and lower boundaries of the model, the model can be regarded as periodic in the y direction and the thermal transport is not affected by the width of the model. The ETC of these ordered porous configurations is calculated as shown in Fig. 2(b). It can be found that the ETC of these configurations has two obvious characteristics. One is that the ETC of the ordered

porous configuration placed in the y direction is significantly higher than that in the x direction. The other is that the clustering form has almost the same effect on ETC in both the x direction and the y direction.

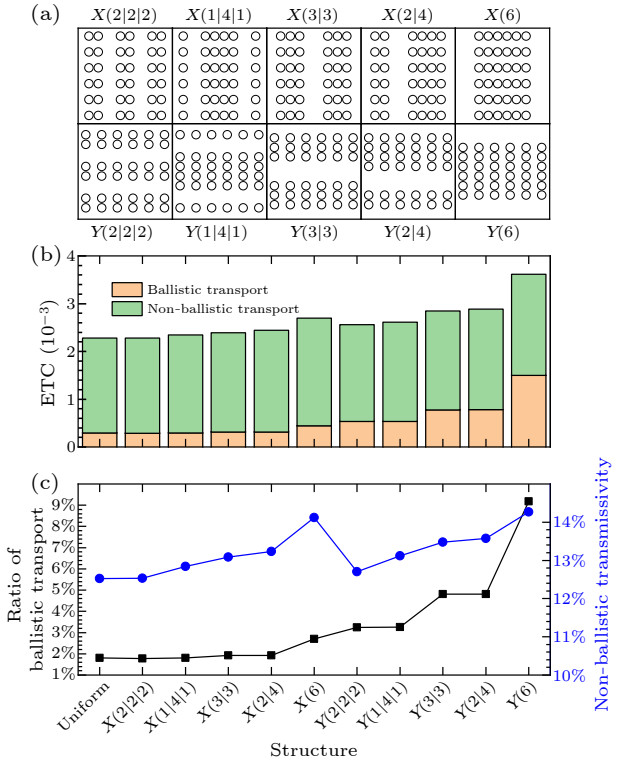

Fig. 2. ETC vs different ordered porous configurations. (a) The ordered porous configuration constructed in the x and y directions, respectively. (b) ETC vs different ordered porous configurations. Here, yellow and green indicate the contribution of ballistic transport and non-ballistic transport, respectively. (c) The ratio of ballistic transport and the non-ballistic transmissivity as functions of the ordered porous configurations.

In order to understand the origin of these characteristics and clarify the scattering mechanism of porous metamaterials, the entire transport process is divided into three sub-processes: ballistic transport process (absorbed by another thermal reservoir and not scattered), non-ballistic transport process (absorbed by another thermal reservoir and scattered), and unsuccessful transport process (absorbed by the emitted thermal reservoir). The proportion of three sub-processes is given in Fig. S2(a) of the Supplementary Material, and it is easy to find that the process with the largest proportion of unsuccessful transport is due to the introduction of the porous structure. In addition, a configuration with a larger ETC corresponds to a smaller probability of an unsuccessful transport process; that is, a larger transmittivity. In addition, as shown in Fig. 2(c), the ratio of the ballistic transport process of the ordered porous configuration placed in the y direction is much higher than that in the x direction, indicating that the compactness in the y direction has an important impact on the ratio of ballistic transport. At the same time, it is easy to find that the configuration with fewer clusters in the y direction has a larger ratio of ballistic transport, which also indicates that the concentration of porous structures strongly affects the ratio of ballistic transport. These ballistic transport processes not only increase the proportion of successful transport processes, but also have a smaller average single-transport time, resulting in a higher ETC, which coincides with the first characteristic mentioned above. On the other hand, the non-ballistic transport process plays a major role in the successful transport process, and its transmittivity is almost irrelevant in terms of the direction of the special configuration, but is closely related to the number of clusters. The more compact the configuration, the greater the transmittivity, which coincides with the second characteristic.

The above conclusions can also be observed from the ETC contributed by different transport processes, as shown in Fig. S2(b). The ETC contributed by ballistic transport has the same increasing trend as the ratio of ballistic transport process. Here, the ETC contributed by ballistic transport in configuration $Y(6)$ is about 100 times higher than that for configuration $X(1|4|1)$, which also indicates that the ratio of ballistic thermal transport in porous materials can be greatly improved by the optimizing configuration to improve ETC. The ETC contributed by non-ballistic thermal transport tends to be the same as the non-ballistic transmittivity, which is almost independent of the direction of the ordered porous configuration. In addition, we also calculate the ETC under different pore sizes and ordered porous configurations, and the results are shown in Fig. S3(a). In the case of different pore sizes, ordered porous configurations show a similar effect and realize the enhancement of ETC in all configurations. At the same time, we also find that in the case of large pores, although the ratio of ballistic transport and the non-ballistic transmissivity are lowest in the uniform configuration, the increase of ETC is the largest in the $Y(6)$ configuration. This is due to the fact that the non-ballistic transmissivity is more affected by the X configuration when the pore size is small, while the ratio of ballistic transport is more favourable to the Y configuration, thus weakening the final increase of ETC.

Furthermore, we also calculate the size effect on the ordered porous configuration and the results are shown in Figs. S4 and S5. When the length and width of the model are doubled simultaneously, ETC decreases significantly, but the ratio of relative change of ETC is abnormally enhanced. The significant reduction of ETC in the uniform configuration is due to the decrease in ballistic and non-ballistic transmissivity induced by the larger model size. However, as the structure becomes more compact, we find that the ballistic and non-ballistic transmissivity almost does not decrease, indicating that an increase in length leads to stronger scattering, but an increase in width also leads to a larger ballistic transport space, and ultimately leads to an abnormal enhancement in the ratio of relative change. Then, when we keep the width unchanged and increase the length, we find that ETC, ballistic and non-

ballistic transmissivity decrease together, but the ratio of relative changes still increases. At this point, we find that as the structure becomes compact, although the ballistic ratio increases slowly, the non-ballistic transmissivity increases faster, because the model is too long to inhibit the ratio of ballistic transport. Fortunately, the ratio of ballistic transport originally brought by the compact structure is transformed into a larger non-ballistic transmissivity. Therefore, the ETC of the model still maintains the original change trend, which also shows that our conclusions are not only applicable to ballistic systems, but also can play a role in diffusion systems.

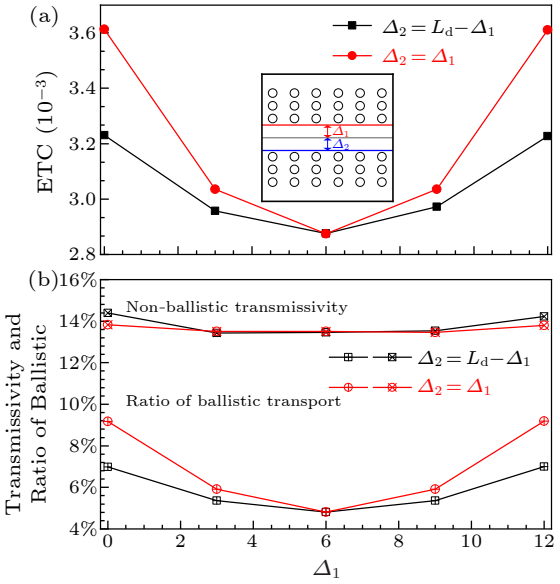

Fig. 3. Asymmetry regulates the thermal transport in the ordered configuration $Y(3|3)$. (a) ETC as a function of asymmetry under translation operation and separation operation. The inset is the schematic diagram on quantitative introduction of asymmetry. (b) The ratio of ballistic transport and non-ballistic transmissivity as functions of asymmetry under translation operation and separation operation.

Different structures correspond to different ratios of ballistic transport and non-ballistic transport transmissivity, which causes great changes in ETC. It is natural to think that if asymmetry is introduced into the ordered structure, can the ETC of porous metamaterials be adjusted further? Here, we take $Y(3|3)$ as an example and introduce two asymmetric operations into it to study the influence of asymmetry on the ballistic thermal transport process in porous metamaterials. As shown in the inset of Fig. 3(a), the two asymmetric operations are as follows: (1) translation operation: to ensure that the distance L_d between the upper and lower two clusters is unchanged and to carry out translation operations on them ($\Delta_2 = L_d - \Delta_1$); (2) separation operation: to ensure that the center of the upper and lower clusters remains stationary and the distance between the clusters ($\Delta_2 = \Delta_1$) can be increased. Here, although the separation operator is symmetric in movement ($\Delta_2 = \Delta_1$), given the periodic boundary conditions in the y direction, the separation operation introduces asymmetry between the upper (or lower) gap and the intermediate gap. Under the action of two asymmetric operations, the ETCs of both two asymmetric $Y(3|3)$ configurations gradually increase. These increases are symmetric around the central position ($\Delta_1 = 6$) and the corresponding results are shown in Fig. 3(a). Here, the asymmetric operation significantly increases the ratio of ballistic transport and the non-ballistic transmissivity, resulting in a larger ETC, as shown in Fig. 3(b). This is due to the fact that the translation operation brings configuration $Y(3|3)$ closer to a larger configuration $Y(3|6)$, and the separation operation brings configuration $Y(3|3)$ closer to a larger and more compact configuration $Y(12)$. Therefore, the separation operation transits the configuration in a more compact direction, causing a large increase in the ratio of ballistic transport, resulting in a more significant improvement in ETC.

Meanwhile, separation operations are also introduced for configurations $X(2|2|2)$ and $Y(2|2|2)$, as shown in Fig. 4(a). Similar to configuration $Y(3|3)$, as shown in Fig. 4(b), the introduction of asymmetry causes ETC to increase significantly, but the increase here is no longer symmetric about the central point. This is due to the fact that, when Δ_{x1} and Δ_{y1} approach 0, configurations $X(2|2|2)$ and $Y(2|2|2)$ gradually change to $X(6)$ and $Y(6)$. When Δ_{x1} and Δ_{y1} approach 12, configurations $X(2|2|2)$ and $Y(2|2|2)$ gradually change to $X(3|6)$ and $Y(3|6)$, which are not as compact as before. Thus ETC changes asymmetrically. Taken together, considering only the configurations $X(2|2|2)$ and $Y(2|2|2)$, the ETC can be regulated from 2.27×10^{-3} to 2.68×10^{-3} by introducing asymmetry, which is close to 20% of the original ETC. At the same time, not only does ETC increase, but the anisotropy of configuration $XY(2|2|2)$ also increases from 1.13 to 1.35.

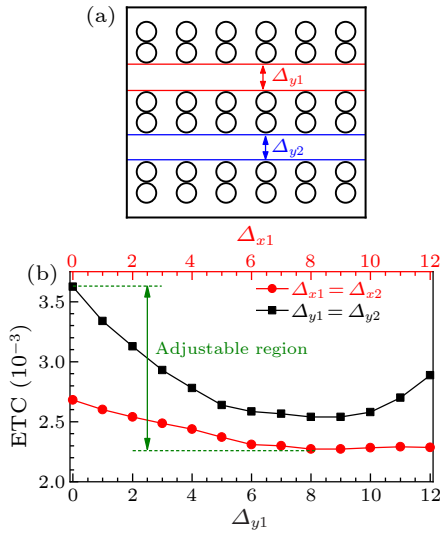

Fig. 4. Asymmetry regulates the thermal transport in the ordered configurations $X(2|2|2)$ and $Y(2|2|2)$. (a) Schematic diagram on quantitative introduction of asymmetry. (b) ETC as a function of asymmetry under separation operation.

To maximize the asymmetry, we introduce disorder into the porous configuration to study the effect of disorder on ballistic thermal transport in porous metamaterials. The uniform configuration is taken as the initial configuration and then the position of each pore is moved randomly. The maximum distance of all pores in both x and y directions is defined as the degree of the disorder δ, as shown in the inset of Fig. 5(a). Here, the maximum degree of disorder is set to 2, because the distance between the pores is 4 in the uniform configuration. For each degree of disorder, 2000 disordered configurations are calculated as shown in Fig. 5(a). With the increase of the degree of disorder, the ETC of the disordered configuration tends to decrease and the broadening of the ETC increases concomitantly.

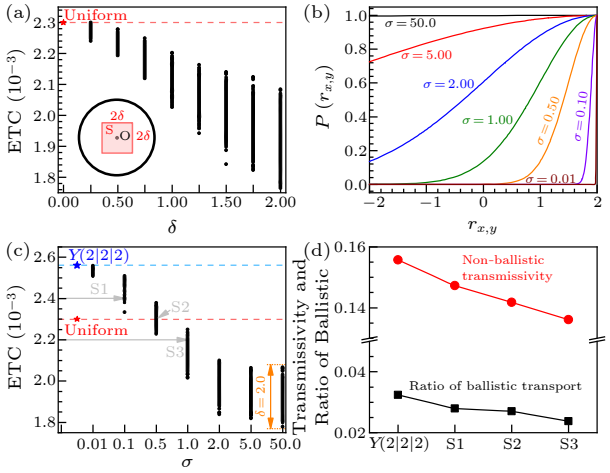

Fig. 5. Disorder regulates the thermal transport in the uniform configuration. (a) Effect of uniform random displacement on ETC of porous metamaterial. The inset is a schematic diagram on quantitative introduction of disorder. (b) Gaussian distribution diagram with different broadenings. (c) Effect of Gaussian random displacement on ETC of porous metamaterial. (d) The ratio of ballistic transport and the non-ballistic transmissivity as functions of disordered configurations.

A total of 16000 disordered configurations are generated and calculated, but no abnormal enhancement configuration is observed. Although no special cases of abnormal enhancement have been observed, this provides a clue as to whether an abnormal enhancement configuration could be seen as resulting from introducing disorder to another more ordered configuration. To confirm this conjecture, we introduce a random displacement $(r_x r_y)$ of Gaussian distribution that tends to cluster the adjacent pores, similar to configuration $Y(2|2|2)$. This Gaussian distribution diagram is shown in Fig. 5(b) and in the following form:

$$P(r_{x,\,y}) = e^{-\frac{(r_{x,\,y}-2)^2}{2\sigma^2}}, \tag{7}$$

where σ is used to describe the dispersion of the Gaussian distribution, which will become uniform and random when it is very large. The ETC of disordered configuration under different Gaussian distributions is shown in Fig. 5(c). When the Gaussian distribution is sharp, a large number of disordered configurations with abnormal enhanced ETC are observed. This indicates that many abnormally enhanced disordered configurations may exist between the uniform configuration and configuration $Y(2|2|)$, which has been observed in macroscopic porous metamaterials.[43] When the Gaussian distribution is very flat, the result behaves exactly as if it is uniformly random. Then, we select three random configurations, S1, S2, and S3, and show the ratio of ballistic transport and the non-ballistic transmissivity in Fig. 5(d). Also, the schematics for the selected configurations are shown in Fig. S6. With the introduction of disorder, the ballistic transport process and the non-ballistic transmissivity decrease simultaneously, leading to a larger average transport time and a more failed transport process, resulting in a significant reduction in ETC.

In conclusion, we have study the ballistic thermal transport process in porous metamaterials by using the Lorentz gas model. In the ballistic transport region, the particles are only scattered by the pores, so the non-ballistic transmissivity and the ratio of ballistic transport play an absolute role in the ETC. Firstly, we study the thermal transport in various ordered configurations and find that the ordered structure perpendicular to the transport direction has a stronger effect on ETC than that parallel to the transport direction. The ETC is obviously enhanced with the decrease of the cluster block. Secondly, when asymmetry is introduced into the ordered structure, the ETC and anisotropy of the porous metamaterial are enhanced. Finally, to maximize the asymmetry, Gaussian disorder can lead to an abnormally increased ETC in porous metamaterials by making the configuration shift to a transition configuration of a more ordered configuration. Our work provides clear theoretical guidance for designs and optimizations of high-performance porous thermal metamaterials in the ballistic thermal transport region.

Acknowledgement. This work was supported by the National Natural Science Foundation of China (Grant Nos. 11975125 and 11890703), and the Department of Science and Technology of Jiangsu Province (Grant No. BK20220032).

References

[1] Waldrop M M 2016 *Nature* **530** 144
[2] Li N B, Ren J, Wang L, Zhang G, Hänggi P, and Li B W 2012 *Rev. Mod. Phys.* **84** 1045
[3] Sklan S R and Li B W 2018 *Natl. Sci. Rev.* **5** 138
[4] Li Y, Li W, Han T C, Zheng X, Li J X, Li B W, Fan S H, and Qiu C W 2021 *Nat. Rev. Mater.* **6** 488
[5] Fan C Z, Gao Y, and Huang J P 2008 *Appl. Phys. Lett.* **92** 251907
[6] Yang Y, Chen H Y, Wang H, Li N B, and Zhang L F 2018 *Phys. Rev. E* **98** 042131
[7] Yang Y, Ma D K, Zhao Y S, and Zhang L F 2020 *J. Appl. Phys.* **127** 195301
[8] Li B W, Wang L, and Casati G 2004 *Phys. Rev. Lett.* **93** 184301
[9] Li B W, Wang L, and Casati G 2006 *Appl. Phys. Lett.* **88** 143501

[10] Yu J K, Mitrovic S, Tham D, Varghes J, and Heath J R 2010 *Nat. Nanotech.* **5** 718
[11] Luckyanova M N, Garg J, Esfarjani K, Jandl A, Bulsara M T, Schmidt A J, Minnich A J, Chen S, Dresselhaus M S, Ren Z F, Fitzgerald E A, and Chen G 2012 *Science* **338** 936
[12] Yu C Q, Ouyang Y L, and Chen J 2022 *Front. Phys.* **17** 53507
[13] Jiang J H, Lu S, and Chen J 2023 *Chin. Phys. Lett.* **40** 096301
[14] Maldovan M 2013 *Phys. Rev. Lett.* **110** 025902
[15] Maldovan M 2015 *Nat. Mater.* **14** 667
[16] Wang H D, Hu S Q, Takahashi K, Zhang X, Takamatsu H, and Chen J 2017 *Nat. Commun.* **8** 15843
[17] Song D and Chen G 2004 *Appl. Phys. Lett.* **84** 687
[18] Hopkins P E, Reinke C M, Su M F, Olsson I R H, Shaner E A, Leseman Z C, Serrano J R, Phinney L M, and El-kady I 2011 *Nano Lett.* **11** 107
[19] Yang L N, Yang N, and Li B W 2014 *Nano Lett.* **14** 1734
[20] Alaie S, Goettler D F, Su M, Leseman Z C, Reinke C M, and El-Kady I 2015 *Nat. Commun.* **6** 7228
[21] Feng T L and Ruan X L 2016 *Carbon* **101** 107
[22] Zhao Y S, Yang L N, Kong L Y, Nai M H, Liu D, Wu J, Liu Y, Chiam S Y, Chim W K, Lim C T, Li B W, Thong J T L, and Hippalgaonkar K 2017 *Adv. Funct. Mater.* **27** 1702824
[23] Wagner M R, Graczykowski B, Reparaz J S, Sachat A E, Sledzinska M, Alzina F, and Torres C M S 2016 *Nano Lett.* **16** 5661
[24] Anufriev R, Ramiere A, Maire J, and Nomura M 2017 *Nat. Commun.* **8** 15505
[25] Oh J, Yoo H, Choi J, Kim J Y, Lee D S, Kim M J, Lee J C, Kim W N, Grossman J C, Park J H, Lee S S, Kim H, and Son J G 2017 *Nano Energy* **35** 26
[26] Hu S Q, Zhang Z W, Jiang P F, Chen J, Volz S, Nomura M, and Li B W 2018 *J. Phys. Chem. Lett.* **9** 3959
[27] Sledzinska M, Graczykowski B, Alzina F, Melia U, Termentzidis K, Lacroix D, and Torres C M S 2019 *Nanotechnology* **30** 265401
[28] Hu S Q, Zhang Z W, Jiang P F, Ren W J, Yu C Q, Shiomi J, and Chen J 2019 *Nanoscale* **11** 11839
[29] Kasprzak M, Sledzinska M, Zaleski K, Iatsunskyi I, Alzina F, Volz S, Torres C M S, and Graczykowski B 2020 *Nano Energy* **78** 105261
[30] Maire J, Anufriev R, Yanagisawa R, Ramiere A, Volz S, and Nomura M 2017 *Sci. Adv.* **3** e1700027
[31] Wei H, Bao H, and Ruan X L 2020 *Nano Energy* **71** 104619
[32] Yang Y, Zhao Y S, and Zhang L F 2023 *Appl. Phys. Lett.* **122** 144102
[33] Lorentz H A 1905 *Proc. K. Ned. Akad. Wet.* **7** 438
[34] Sinai Y G 1979 *Funct. Anal. Appl.* **13** 192
[35] Bunimovich L A and Sinai Y G 1980 *Commun. Math. Phys.* **78** 247
[36] Bunimovich L A and Sinai Y G 1981 *Commun. Math. Phys.* **78** 479
[37] Oliveira D F M, Vollmer J, and Leonel E D 2011 *Phys. D (Amsterdam)* **240** 389
[38] Moran B, Hoover W G, and Bestiale S 1987 *J. Stat. Phys.* **48** 709
[39] Larralde H, Leyvraz F, and Mejia-Monasterio C 2003 *J. Stat. Phys.* **113** 197
[40] Alonso D, Artuso R, Casati G, and Guarneri I 1999 *Phys. Rev. Lett.* **82** 1859
[41] Li B W, Casati G, and Wang J 2003 *Phys. Rev. E* **67** 021204
[42] Chen H Y, Wang H, Yang Y, Li N B, and Zhang L F 2018 *Phys. Rev. E* **98** 032131
[43] Casati G, Mejia-Monasterio C, and Prosen T 2007 *Phys. Rev. Lett.* **98** 104302
[44] Chen H Y, Yang Y, Yu Z Z, Zhong M, and Zhang L F 2020 *Phys. Rev. E* **101** 042129
[45] Yang Y, Li X L, and Zhang L F 2021 *Chin. Phys. Lett.* **38** 016601
[46] Wu Y C, Yang Y, Lu L K, Wang T T, Xu L, Yu Z Z, and Zhang L F 2021 *Phys. Rev. E* **103** 052135
[47] Wang H, Yang Y, Chen H Y, Li N B, and Zhang L F 2019 *Phys. Rev. E* **99** 062111
[48] Wang T T, Yang Y, Wu Y C, Xu L, Ma D K, and Zhang L F 2021 *Phys. Rev. E* **104** 024801